



Mechanical Damage Induced by the Water–Rock Reactions of Gypsum-Bearing Mudstone

Shifei Ping^{1,2,4} · Fugang Wang^{1,2,5} · Donghui Wang³ · Shengwei Li³ · Yaohui Wang^{1,2} · Yilong Yuan^{1,2} · Guan hong Feng^{1,2}

Received: 30 October 2023 / Accepted: 9 March 2024 / Published online: 4 April 2024
© The Author(s), under exclusive licence to Springer-Verlag GmbH Austria, part of Springer Nature 2024

Abstract

The deterioration of the mechanical properties of gypsum due to water–rock reactions has attracted extensive attention in the areas of structural geology and civil engineering, and accurately predicting variations in the mechanical behavior of gypsum under different engineering conditions presents a challenging yet intriguing endeavor. In our study, we conducted experimental investigations of the influence of water–rock reactions on the mechanical behavior and mechanisms of gypsum-bearing mudstone. Subsequently, we constructed a mechanical damage model to predict the behavior under varying dissolution times. During the water–rock reaction, water dissolves substances along crystal interfaces and mineral joint surfaces, changing the way particles contact each other, weakening the contact strength, creating intergranular solubility pores, and causing an increase in porosity, all of which lead to a decrease in the mechanical strength of gypsum-containing rocks. The experimental results showed that the maximum decrease in peak strength and cohesion of the samples with the increase in porosity was 69.68% and 79.02% after the water–rock reaction, respectively, and the internal friction angle showed a small fluctuation change with increasing porosity. The maximum increase in elastic modulus and peak strength with increase in confining pressure was 34.21% and 37.10%, respectively. In addition, for samples with different shapes and spatial locations of weak zones due to water–rock reactions, there is no clear relationship between the change of elastic modulus and the porosity of the samples. By constraining the peak strength and peak deformation, the established gypsum-bearing mudstone constitutive model was accurate and flexible. Comparing the established damage constitutive model with measurements, we found that the developed damage constitutive model is compatible with the measured data during the damage evolution process of water–rock reactions over long periods and can play a predictive role. This study has laid an important foundation for research on the evolution of gypsum mechanical properties and model construction under water–rock reactions.

Highlights

- Extensive indoor dissolution tests and mechanical tests are conducted.
- The damage mechanism of gypsum-bearing mudstone under water–rock reactions is explored.
- The variation of rock mechanical parameters under water–rock reactions is obtained.
- A widely applicable constitutive model is developed

✉ Fugang Wang
wangfugang@jlu.edu.cn

¹ Key Laboratory of Groundwater Resources and Environment, Ministry of Education, Jilin University, Changchun 130012, China

² Jilin Provincial Key Laboratory of Water Resources and Environment, Jilin University, Changchun 130012, China

³ Chengdu Center, China Geological Survey, Chengdu 610081, China

⁴ Yellow River Institute of Hydraulic Research, Yellow River Conservancy Commission, Zhengzhou 450003, China

⁵ Present Address: 2519#, Jiefang Road, Chaoyang District, Changchun 130012, China

Keywords Water–rock reactions · Damage mechanisms · Rock strength · Rock deformation characteristics · Constitutive model

1 Introduction

Gypsum, as an evaporite mineral, plays an important role in several areas, such as structural geology and civil construction. It affects basin dynamics, involves orogeny, and is associated with many economic activities, including mining, waste repositories, and oil exploration (Cristallini and Ramos 2000; Zucali et al. 2010; Liang et al. 2012; Lisabeth and Zhu 2015). In particular, underground engineering excavations in gypsum have often resulted in land subsidence, pillar failures, and water gushing (Bajni et al. 2019; Song et al. 2018; Noémie, et al. 2016), especially after unexpected groundwater circulation (Bonetto et al. 2008; Sadeghiamirshahidi and Vitton 2019). Unlike widely available carbonates (Baud et al. 2016), gypsum is typically characterized by high solubility and low mechanical strength (Miao et al. 2016). As such, the mechanical properties of gypsum are susceptible to the presence of groundwater, which may cause important weakening and weathering effects (Brantley and Conrad 2008; Juang 2021; Criss and Nelson 2020; Liu et al. 2020).

It is effective for the prevention of geologic disasters to clarify the variation of mechanical behavior of gypsum-bearing rocks in the water–rock reaction (Juang 2021). An accurate assessment of variation of gypsum mechanical parameters under water–rock reactions is the basis for predicting the mechanical behavior of gypsum (Miao et al. 2016). In recent decades, researchers have endeavored to explore the effects of different water saturation levels, different soaking times, and different soaking solutions on the mechanical behavior of gypsum, including elastic modulus, triaxial compressive strength, and tensile strength (Hoxha et al. 2006; Adams et al. 2019; Zhu et al. 2019; Işık 2010). It was observed that these were some consistencies in these mechanical parameters, and the presence of groundwater weakened all the mechanical parameters. Limited by the difficulty of sample preparation, few studies have revealed the variation of the key mechanical parameter (cohesion and internal friction angle) with water–rock reaction time (Bertotti and Mosca 2009). Moreover, under different geological structures and different buried depths, the ground stress of gypsum-bearing rocks is different, and different from the influence of water–rock reaction on the deterioration of mechanical parameters of gypsum-bearing rock, ground stress has a significant promoting effect on rock mechanical parameters (Nol et al. 2021; Envelope et al. 2022). Under the coupling effect of ground stress and water–rock reaction, the

variation of mechanical parameters of gypsum-bearing rock is not clear, which is extremely unfavorable to the construction of underground engineering excavations.

The constitutive relation is a mathematical expression of the variation of rock mechanical behavior (Homand 2005), and establishing rock constitutive relations is an important method to better understand and predict the strength and deformation of rocks during water–rock reactions (Li et al. 2021; Barbero and Vivo 2001; Ma et al. 2021a; Wong and Einstein 2009; Gao et al. 2021). Gypsum-bearing rocks in nature is a natural geological body with natural microdefects such as pores and microfractures at different scales (Zhu et al. 2022). These microdefects gradually develop and combine under the action of external loads and groundwater, not only causing macroscopic cracks in the rock, but also gradually deteriorating the strength and deformation properties of the rock mass (Liu, et al. 2016; Gong et al. 2019). Therefore, the method based on statistical damage mechanics, which is an attractive tool to describe the deformation damage of rock, has been successfully applied to the construction of rock damage constitutive models with abundant results (David et al. 2012; Liu and Dai 2018). Zhu et al. (Zhu et al. 2019) established a damage constitutive model for soaking softening of gypsum-containing rocks over time. Ma et al. (Ma et al. 2021b) established a damage constitutive model of gypsum-bearing rocks based on the theory of energy dissipation. Lin et al. (Yun et al. 2019) established a mechanical damage constitutive model considering chemical dissolution based on statistical damage mechanics. However, few investigations on constitutive models of rocks during water–rock reactions have been conducted. The form of the rock mechanics model depends mainly on the type of rock. Owing to the structural complexity of gypsum-bearing rocks (Meng et al. 2016), it is very challenging to model the mechanical damage of gypsum-bearing rocks in water–rock reactions. In addition, most existing studies have taken the corresponding conditions when the axial strain reaches a specified value as the extreme value point by assumption, but these conditions restrict the application of the constitutive model and hinder generality.

The profound cause behind the variations in the mechanical behavior of gypsum-bearing rock during water–rock reactions lies in the alteration of both macro- and microstructures of the rock. It is the basis of constitutive model construction to clarify the change process of macro- and microstructure of gypsum-bearing rock and to carry out quantitative characterization (Wang et al. 2017).

Surprisingly, even though the change of macro- and micro-structure of pure synthetic gypsum is well known because of its use as homogeneous artificial rock, little is known about the change of macro- and microstructure of natural gypsum rock.

The distribution area of gypsum in the Sichuan Basin and its margins is about 165,000 km², accounting for 1.718% of the China's land area (Ping 2023). In recent years, with economic development, the demand for underground space utilization is increasing and a series of underground projects (such as subway, shopping malls, and underground power stations) will be constructed in Chengdu Tianfu New Area. Under natural conditions, the groundwater flow in the area is stagnant, and gypsum erosion is nearly in a saturated state. However, under the disturbance of underground engineering, especially the process of engineering dewatering, the dynamic characteristics of groundwater will be significantly changed, inducing drastic gypsum erosion. The deterioration of the mechanical properties of gypsum-bearing strata under the engineering disturbances cannot be ignored.

In this study, using a field-obtained natural gypsum-bearing mudstone as a research object, we explored the change mechanism and variation of rock mechanical properties under the influence of water–rock reaction and constructed a constitutive model with wider applicability. The novelty of this paper includes the following three aspects: (1) the microstructural and macrostructural variations of gypsum-bearing mudstones during water–rock reaction are systematically revealed; (2) the variation rules of the gypsum-bearing mudstone mechanical parameter (e.g., elastic modulus, peak strength, cohesion, and internal friction angle) are investigated, and the mathematical expression of the peak strength coupled with the confining pressure and dissolution is constructed; (3) the quantitative expression of the macroscopic structural change process of the samples is realized through the testing of the porosity of the samples, and the mechanical constitutive model of a wide range of applicability is constructed on the basis of this model. Our research results are of great significance in guiding the construction of underground projects in Chengdu and can provide a reference for the evolution of mechanical properties of gypsum-bearing mudstone under water–rock reaction.

2 Materials and Methods

2.1 Rock Sample Preparation

The core samples were collected from gypsum mudstone of the Cretaceous Guankou Formation in Tianfu New area with a depth of 40–100 m (Fig. 1a), Chengdu, China.

The main strata of the study area is composed of Jurassic Penglai Formation sandstone, Cretaceous Jiaguan Formation siltstone, Cretaceous Guankou Formation mudstone, and clay and pebble layers of the Quaternary Holocene and Middle Pleistocene. According to international rock mechanics test standards, 57 standardized samples were processed (Fig. 1b). Since it was important to ensure the homogeneity of the test samples, 30 samples were selected with the same burial depth, the same gypsum surface distribution pattern, and similar densities (Fig. 1c). From the XRD test results, the mineral composition of the sample was obtained (Fig. 1d).

2.2 Experimental Apparatus

A 1 L wide-mouth bottle was used for indoor dissolution test.

The HK automatic pore osmotic coupling tester was used for porosity testing. According to Boyle's law, a closed chamber containing the test sample is filled with nitrogen and the volume of nitrogen is recorded, at which time the gas expands isothermally within the chamber at atmospheric pressure and fills the pores inside the test sample. The pore volume V_p and particle volume V_s of the rock sample are calculated. The porosity of a rock sample can be expressed as

$$\phi = \frac{V_p}{V_p + V_s}, \quad (1)$$

where ϕ is the porosity, V_p is the pore volume, and V_s is the particle volume.

Rock mechanics testing was performed using a TAW-2000 triaxial pressure testing machine, which is composed of an axial loading system, confining pressure system, heating system, and computer system. The maximum confining pressure and maximum axial pressure are 100 kN with an error of 1% and 200 kN with an error of 0.5%.

2.3 Experimental Procedure

Laboratory experiments were a common means of investigating variations in rock mechanical properties under water–rock reactions. Here we have conducted indoor dissolution tests and mechanical tests, which we will discuss separately. The detailed experimental procedure can be found in our pre-publication literature (Ping 2023), which has been somewhat simplified here.

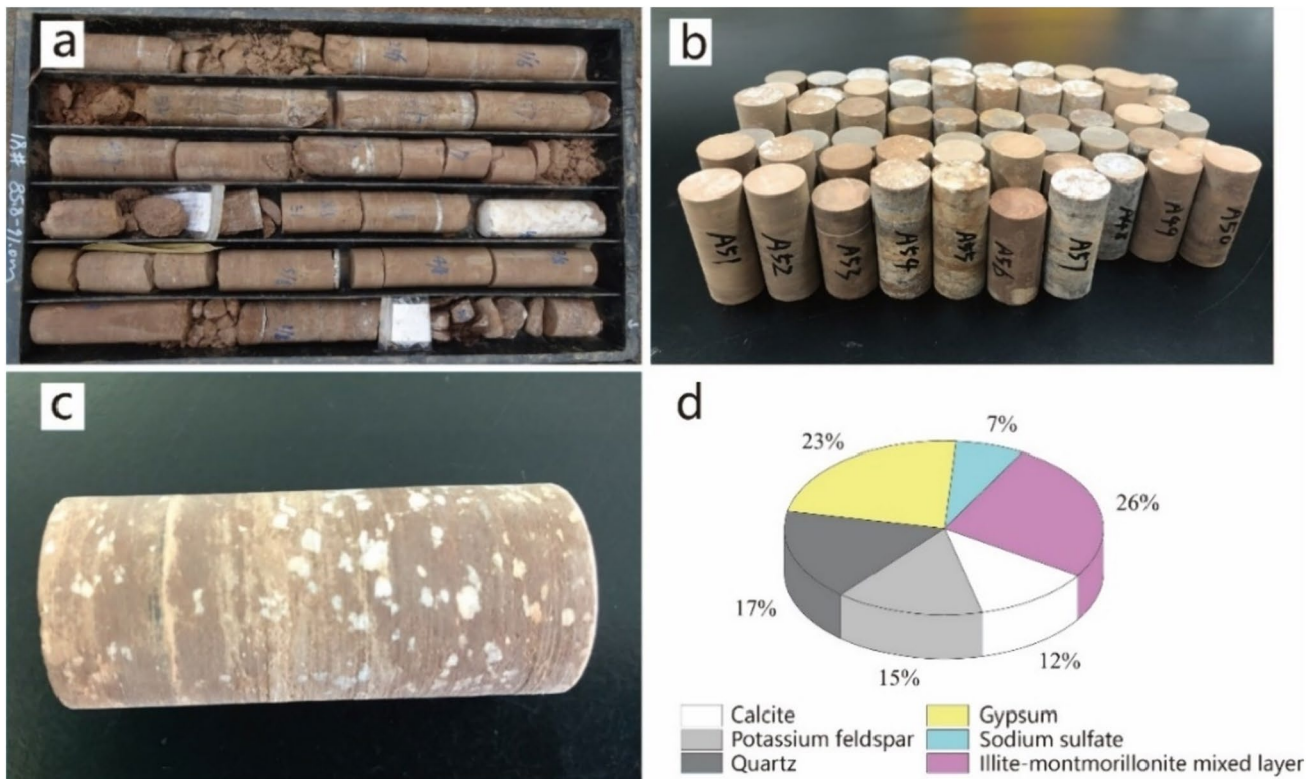


Fig. 1 Field cores (a); standard samples (b); test samples (c); mineral volume fraction (d)

2.3.1 Indoor Dissolution Test

The experimental conditions were determined according to the conditions of the study area. Groundwater in the study area was mostly neutral water and flowed at 3.12×10^{-8} – 1.08×10^{-6} cm/s. The water temperature was 19–25 °C. Atmospheric precipitation is the main recharge source of groundwater in the upper layers of the stratum, and the infiltration of submerge causes the dissolution of gypsum in the stratum. Therefore, we used neutral distilled water instead of phreatic water, and the dissolution experiment temperature was set to 20 °C. In accordance with international rock mechanics testing requirements, the field-obtained cores were processed into 57 standardized samples, from which 30 samples with uniform texture and similar distribution of gypsum morphology were selected for testing. Please refer to the literature for more detailed test procedures (Ping 2023). The dissolution times were 1, 3, 6, 10, and 15 days. There were six groups containing five standard samples per group. Table 1 lists the sample size and details of the experimental scheme.

We tested the drying mass m_1 , porosity ϕ_0 , and microscopic crystal structure of the samples before dissolution, and then conducted indoor dissolution tests to test the mass m_2 , porosity ϕ_1 , and microscopic crystal structure of the specimens after dissolution for different

times; please refer to the literature for more detailed test procedures (Ping 2023).

2.3.2 Mechanical Testing

The rock samples after the water–rock reaction were subjected to mechanical tests; the axial displacement was determined by means of a displacement sensor with an accuracy of 1%. Due to the lack of measured ground stress data, the testing confining pressure (Table 1) was set up considering the sampling depth of about 100m and the gravity stress of formation of about 3MPa, as well as considering the extreme conditions. Please refer to the literature for more detailed test procedures (Ping 2023).

3 Results and Discussions

3.1 Experimental Results

3.1.1 Changes in Sample Physical Properties

Table 2 lists the experimentally obtained physical properties of samples before and after dissolution. After dissolution, the percentage of mass loss of the samples was between 0.37% and 4.19%. Hence, the mass of the sample decreased

Table 1 Experimental scheme

Sample size and grouping								Confining pressure (MPa)
	Group code/ (dissolution time/day)	Diameters (cm)	High (cm)		Group code (dissolution time/day)	Diameters (cm)	High (cm)	
Group 1 (1 day)	A1	2.459	4.944	Group 2 (3 days)	A6	2.507	5.130	0.1
	A2	2.479	5.015		A7	2.508	4.957	2
	A3	2.502	4.922		A8	2.487	4.953	3
	A4	2.499	4.994		A9	2.492	4.901	4
	A5	2.504	4.988		A10	2.518	5.062	5
Group 3 (6 days)	A11	2.510	5.143	Group 4 (10 days)	A16	2.483	4.628	0.1
	A12	2.511	5.130		A17	2.488	5.041	2
	A13	2.483	5.038		A18	2.477	4.946	3
	A14	2.457	4.996		A19	2.471	5.099	4
	A15	2.484	5.194		A20	2.499	5.013	5
Group 5 (15 days)	A21	2.496	4.986	Group 6 (natural state)	A26	2.476	5.177	0.1
	A22	2.506	4.486		A27	2.446	5.107	2
	A23	2.479	5.022		A28	2.414	5.212	3
	A24	2.475	5.140		A29	2.491	4.850	4
	A25	2.459	5.108		A30	2.466	5.154	5

substantially, with a maximum decrease of 2.353 g. The porosity of the samples was between 0.1024 and 0.1537, and the porosity increased considerably, with a maximum increase of 0.0533.

3.1.2 Mechanical Tests

Figure 2 shows the stress–strain curves of rock samples after different dissolution times. In the initial state, when the confining pressure reaches 5 MPa, the sample had the highest peak strength of 41.54 MPa. After 15 days of dissolution, the lowest peak strength of the sample was 7.21 MPa under a confining pressure of 0.1 MPa. The peak strength of the samples was significantly reduced due to the water–rock reactions, and the peak strength gradually increased with increasing confining pressure.

3.2 Effects of Water–Rock Reaction on Mechanical Properties

The water–rock reactions were the inducing factor for changes in the pore structure, altering the mechanical parameters as a macroscopic expression (Niu et al. 2022). To facilitate the analysis and construction of a mechanical model, we chose porosity as a variable to measure the damage of rock samples by water–rock reactions. In addition, to eliminate the influence of sample variability on the experimental results, we averaged porosity φ_c of each group across the five samples in

each group (Table 3). Then, we analyzed the deterioration in rock mechanical properties undergoing water–rock reactions through the evolution of mechanical parameters of rock samples with different porosities.

3.2.1 Macrostructure and Microstructure Evolution

(1) Macrostructure evolution

Figure 3 illustrates the macrostructural changes in the samples at different water–rock reactions times. Here, we only show the surface structure characteristics of a typical specimen at each dissolution time. The surface of the gypsum-bearing mudstone in its natural state is relatively flat and smooth, with locally distributed microfractures. The gypsum minerals are distributed between the skeleton (Fig. 3a). After 1 day of dissolution, the surface of the specimen was dissolved to form small grooves with local exposure of gypsum crystals (Fig. 3b). On 3–6 days of dissolution, the samples' surface grooves gradually develop internally, forming a network of local fractures and large dissolution pores (Fig. 3c, d). On 10–15 days of dissolution, a network of fractures and dissolution pores appears over the entire surface of the samples, and gradually develops internally, with large areas of exposed gypsum crystals (Fig. 3e, f).

The emergence of macroscopic weak zones (e.g., dissolution pores and fractures) is the result of vari-

Table 2 Physical parameters of rock samples

Group/sample	Group 1 (1 day)					Group 2 (3 days)				
	A1	A2	A3	A4	A5	A6	A7	A8	A9	A10
m_1 (g)	54.057	54.915	54.911	54.027	55.164	55.454	55.710	55.340	55.235	55.155
Φ_0 (%)	11.51	9.66	10.22	10.17	9.65	10.96	10.18	9.72	9.95	9.97
m_2 (g)	53.855	54.535	54.477	53.836	54.901	54.909	55.170	54.840	54.713	54.613
Φ_1 (%)	12.02	10.24	10.61	10.62	10.64	11.78	11.72	11.72	12.25	11.29
Δm (g)	-0.202	-0.380	-0.434	-0.191	-0.263	-0.545	-0.540	-0.500	-0.522	-0.542
$\Delta\Phi$ (%)	+0.51	+0.58	+0.39	+0.45	+0.99	+0.82	+1.54	+2.00	+2.30	+1.32
Group/sample	Group 3 (6 days)					Group 4 (10 days)				
	A11	A12	A13	A14	A15	A16	A17	A18	A19	A20
m_1 (g)	55.996	55.459	56.993	56.053	55.685	54.674	55.900	55.173	54.120	57.023
Φ_0 (%)	10.32	9.89	10.01	9.74	10.01	11.21	11.69	9.63	10.48	9.83
m_2 (g)	55.272	54.602	56.178	55.386	54.130	52.541	54.244	53.857	52.450	56.006
Φ_1 (%)	12.38	12.75	12.16	11.47	12.87	14.43	14.75	13.64	15.12	14.52
Δm (g)	-0.724	-0.857	-0.815	-0.667	-1.555	-2.133	-1.656	-1.316	-1.670	-1.017
$\Delta\Phi$ (%)	+2.06	+2.86	+2.15	+1.73	+2.86	+3.22	+3.06	+4.01	+4.64	+4.69
Group/sample	Group 5 (15 days)					Group 6 (Natural state)				
	A21	A22	A23	A24	A25	A26	A27	A28	A29	A30
m_1 (g)	56.153	56.151	56.122	56.265	55.474	56.355	55.162	55.487	55.256	55.134
Φ_0 (%)	10.35	9.45	9.57	10.31	11.69	9.67	10.05	10.16	9.88	10.36
m_2 (g)	54.250	53.798	54.465	54.639	53.775	-	-	-	-	-
Φ_1 (%)	14.78	14.78	14.52	15.37	13.57	-	-	-	-	-
Δm (g)	-1.903	-2.353	-1.657	-1.626	-1.699	-	-	-	-	-
$\Delta\Phi$ (%)	+4.43	+5.33	+4.95	+5.06	+1.88	-	-	-	-	-

Note: m_1 and Φ_0 are the sample mass and porosity before dissolution, respectively, while m_2 and Φ_1 are the sample mass and porosity after dissolution, respectively; Δm and $\Delta\Phi$ are the amount of mass change and porosity change, respectively

ous physical changes of the samples (e.g., no reaction particles falling off, lubricated and softened interfaces between particles, redox reactions, swelling of nonreaction minerals, dissolution/precipitation reactions, and ion exchange). At the same time, the shape and spatial location of the weak areas on the surface of different samples at the same dissolution time may have different effects on the mechanical parameters of the samples (Sammis and Ashby 1986).

(2) Microstructure evolution

Water–rock reactions deteriorate the mechanical strength and deformation properties of rocks, and irreversible changes in microscopic grains of rocks are constitutive to the deterioration of mechanical properties (Wei et al. 2015; Yao et al. 2020, 2023). Changes in the internal microstructure during water–rock reactions are driving forces for the deterioration of rock strength and deformation properties (Voyiadjis and Kattan 2009).

Figure 4 shows the scanning electron microscopy images of rock samples with different water–rock reaction times. To highlight the changes of the sample structure by the dissolution of soluble minerals in the process of dissolution, we chose the location with a large degree of dissolution to carry out SEM observation. Before dissolution, the surface of the sample was relatively complete, with clear characteristics of vertical fractures and layered bedding, and face-to-face contact between particles (Fig. 4a). After dissolution (Fig. 4b–e), pores appeared on the surface of the samples, and the particle connection gradually changed to curve-to-curve contact. In addition, intergranular dissolved pores began to appear on the surface of the samples. After 15 days of dissolution (Fig. 4f), with the development and growth of intergranular dissolved pores, intergranular fracture appeared on the surface of the samples.

In summary, we consider that the main effects of water–rock reactions on the microstructure of gypsum-bearing mudstones are the following:

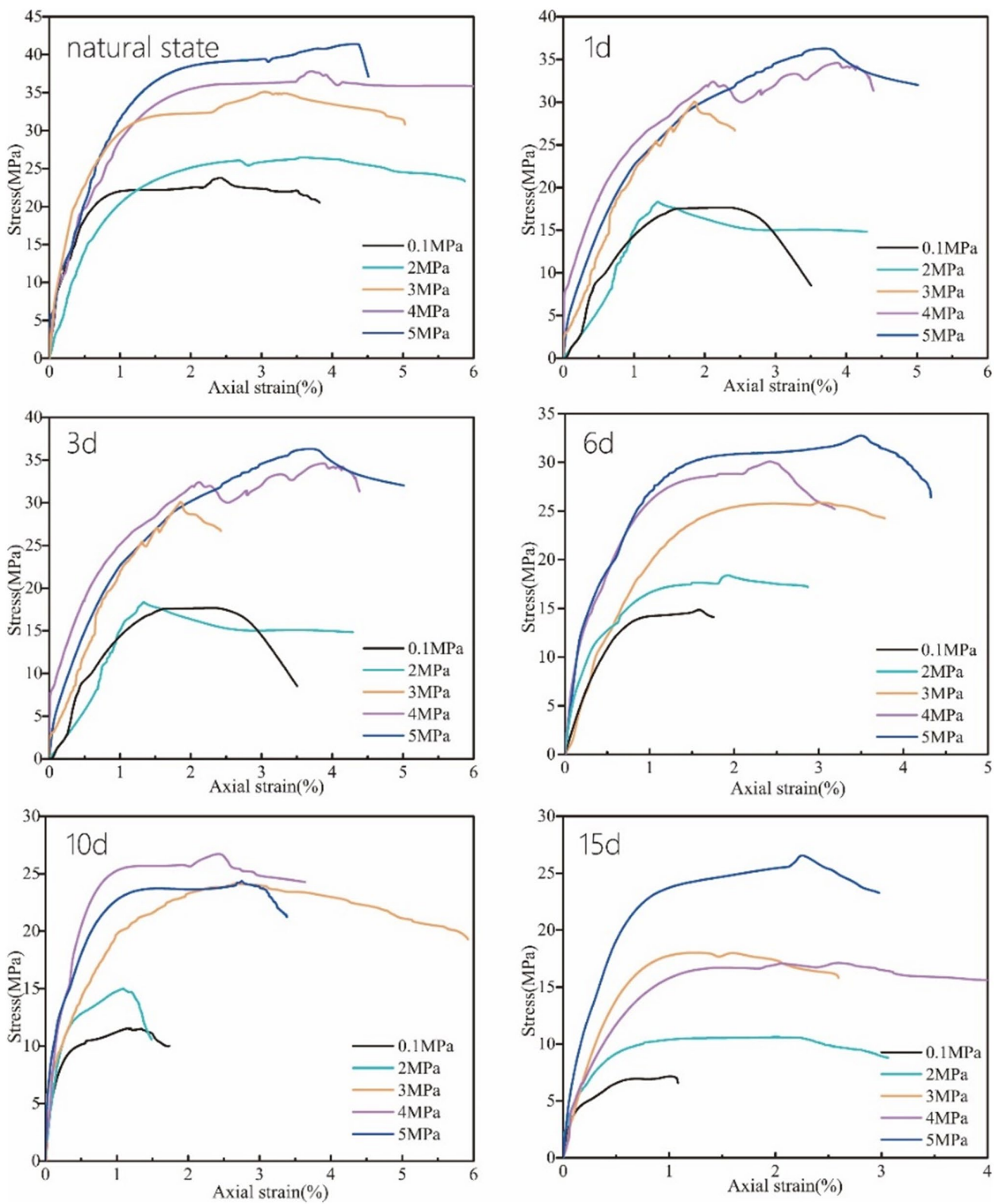
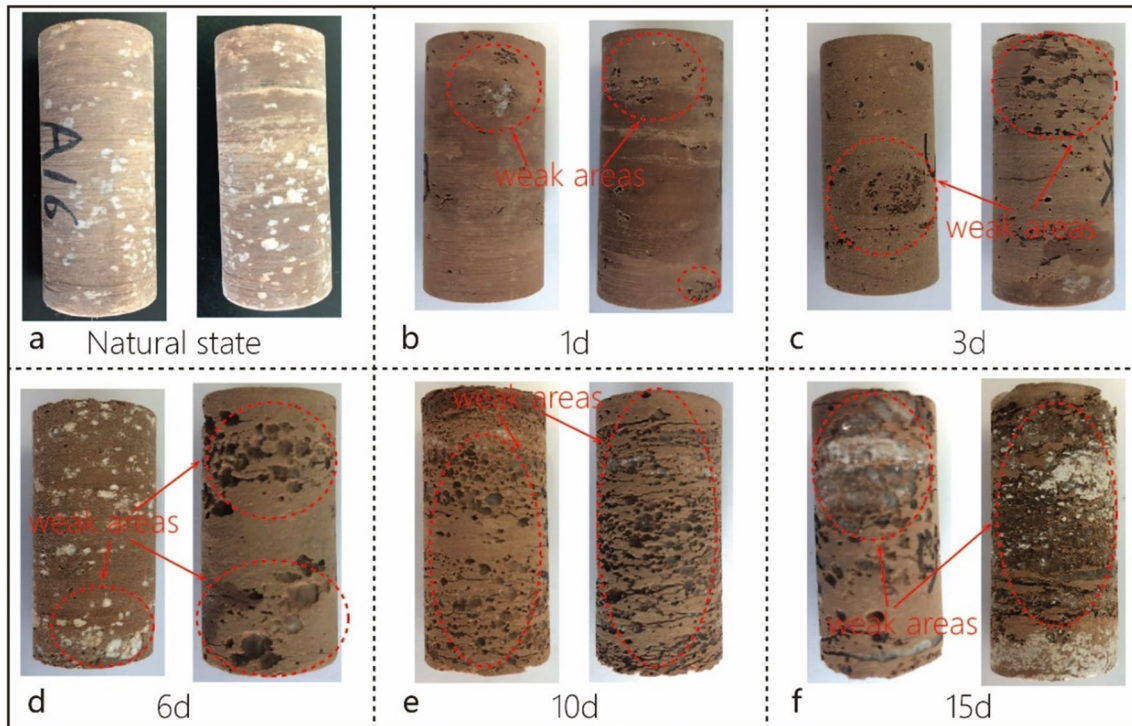


Fig. 2 Stress–strain curves of samples during water–rock reactions.³⁸

Table 3 Average porosity per group of samples

Group	Group 1	Group 2	Group 3	Group 4	Group 5	Group 6
Porosity φ_c (%)	10.83	11.75	12.33	14.49	14.60	10.25

**Fig. 3** Macrostructure characteristics of samples at different dissolution times

- (1) Changed the type of contact between particles: the contact between particles gradually changes from face-to-face contact to curve-to-curve contact.
- (2) Weakens the strength of the contact between the particles: some particles gradually fall off as the reaction proceeds.
- (3) Generation of microdefects such as intergranular dissolved pore and intergranular fracture.

3.2.2 Peak Strength and Peak Deformation Variation with Water–Rock Reaction Time

We defined peak strength σ_p as the stress at the highest point of the stress–strain curve. Figure 5a shows the variation of peak strength of rock samples with confining pressure. Under different water–rock reaction times, the peak strength of the rock samples gradually increased with higher confining pressures in a nonlinear variation. When the confining pressure increased from 0.1 MPa to 5 MPa, the increase in peak strength of the rock samples was 17.64 MPa under natural conditions and 18.76 MPa, 17.07 MPa, 17.75 MPa, 12.88 MPa, and 19.61 MPa after 1, 3, 6, 10, and 15 days

of water–rock reactions, respectively. Figure 5b shows the evolution of the peak strength of the rock samples according to porosity φ_c . Under the same confining pressure, the peak strength of the sample decreased linearly and gradually with increasing porosity φ_c . For porosity φ_c increasing from 0.1083 to 0.1460 and confining pressures of 0.1 MPa, 2 MPa, 3 MPa, 4 MPa, and 5 MPa, the drop in peak strength of the rock samples was 16.57 MPa, 15.82 MPa, 17.50 MPa, 19.17 MPa, and 14.60 MPa, respectively.

It can be concluded that water–rock reactions substantially deteriorate the peak strength of the rock. With the dissolution of gypsum, the porosity φ_c of the samples increased and the volume of the sample skeleton decreased (Fig. 3b–f), resulting in a decrease in the peak strength of the samples. In addition, the confining pressure provided a considerable gain in the peak strength of the rock. With increasing confining pressure, the native pores and pores generated by mineral dissolution inside the rock gradually shrank, and the peak strength of the rock samples gradually increased.

By fitting with the experimental data, we obtained a fitting formula for the peak strength of the samples. Based on the established model, the peak strengths of the rock

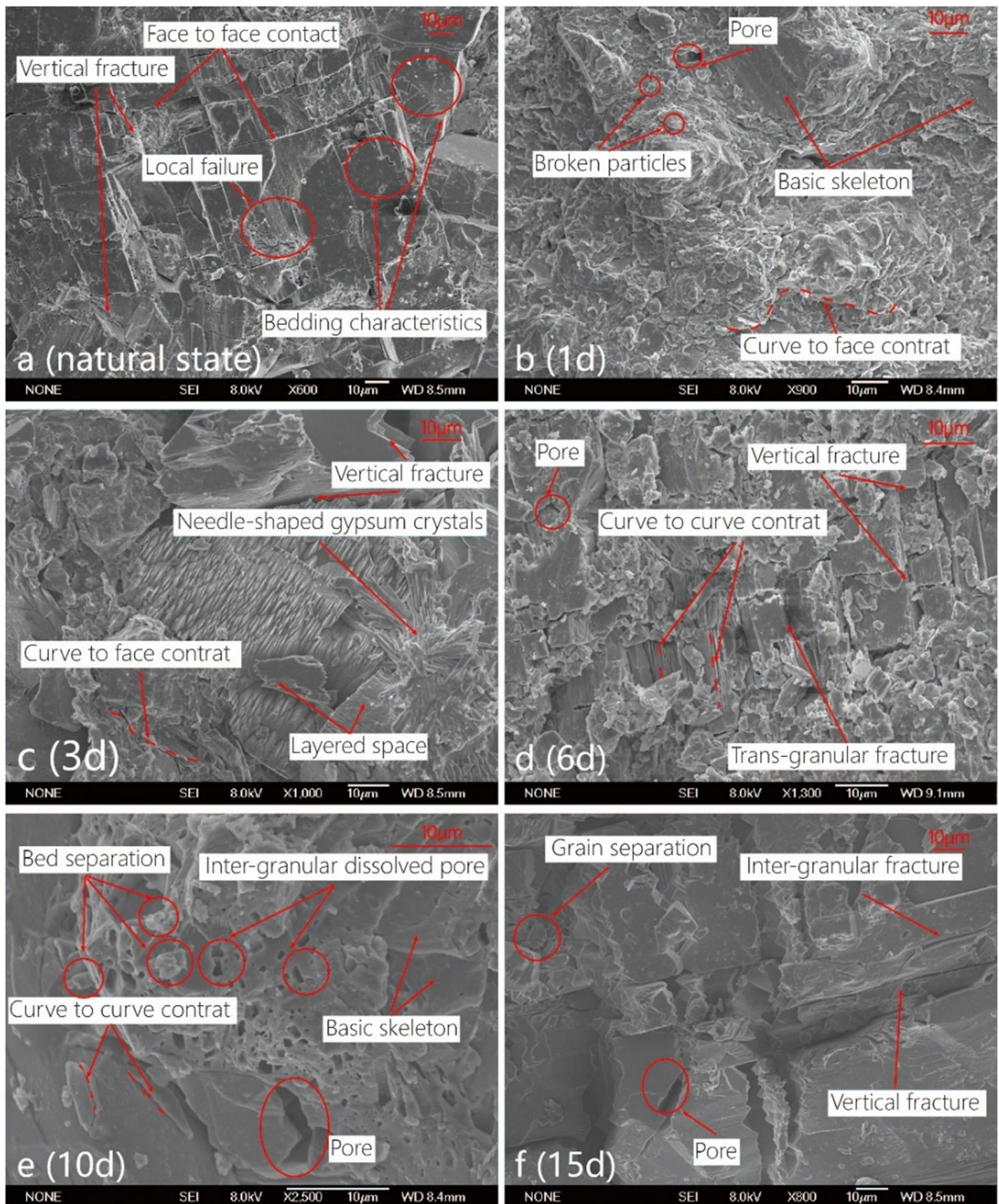


Fig. 4 Microstructure characteristics of samples at different dissolution times

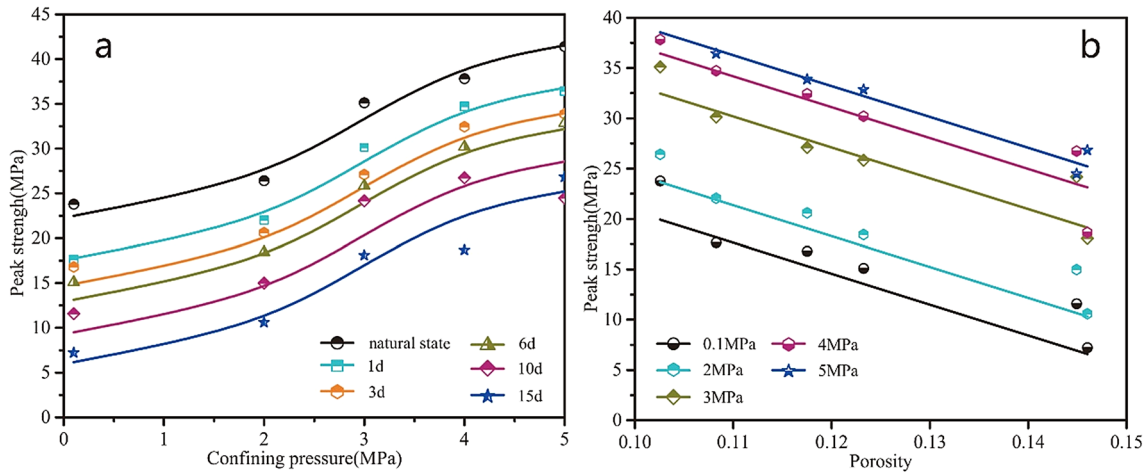


Fig. 5 Peak strength of samples according to confining pressure and porosity

samples under different confining pressures, σ_3 , and porosities, ϕ_c , were predicted and compared with the actual values (Fig. 5), obtaining a suitable fitting effect through the following expression:

$$\sigma_p(\phi_c, \sigma_3) = -306.72\phi_c - 0.51\sigma_3^3 + 4.22\sigma_3^2 - 4.52\sigma_3 + 51.37. \tag{2}$$

Peak strain ϵ_p corresponds to the peak strength of the rock. Figure 6a shows the peak strain of rock samples under confining pressures of 0.1 MPa, 1 MPa, 2 MPa, 3 MPa, 4 MPa, and 5 MPa. Under different water–rock reaction times, the peak strain increased gradually with increasing confining pressure. Figure 6b shows the peak strain of rock samples with porosity. Under the same confining pressure, the peak strain decreased gradually with increasing porosity (Li et al. 2021).

Figure 6 shows that the peak strain has a linear relationship with both the confining pressure and porosity. The relation between the peak strain and both confining pressure σ_3 and porosity ϕ_c can be expressed as:

$$\epsilon_p = 0.3665\sigma_3 - 35.635\phi_c + 6.1725. \tag{3}$$

3.2.3 Elastic Modulus Variation with Water–Rock Reaction Time

The elastic modulus refers to the tangent modulus determined from the linear segment between 40 and 60% of the peak stress along the stress–strain curve under a certain confining pressure. Figure 7a shows the elastic modulus of rock samples according to the confining pressure. Under

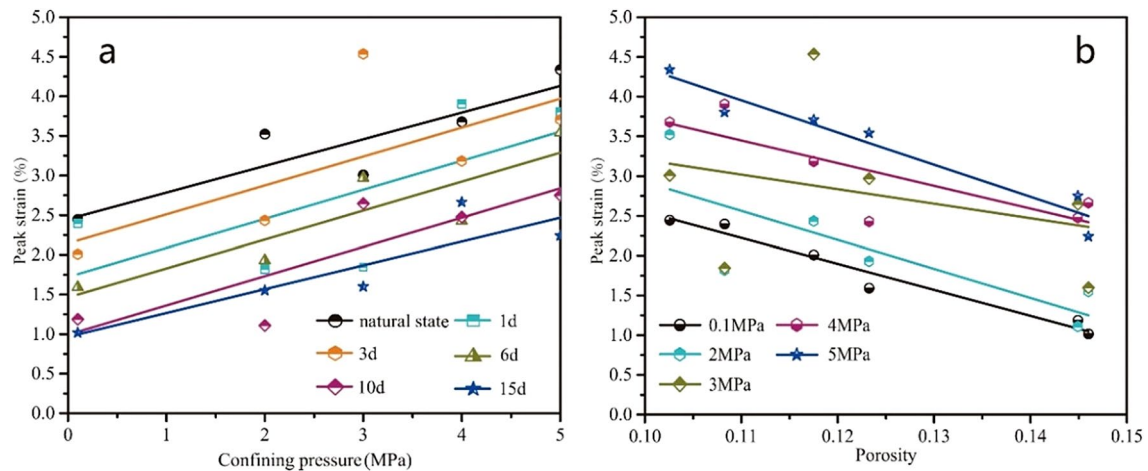


Fig. 6 Peak strain of samples according to confining pressure and porosity

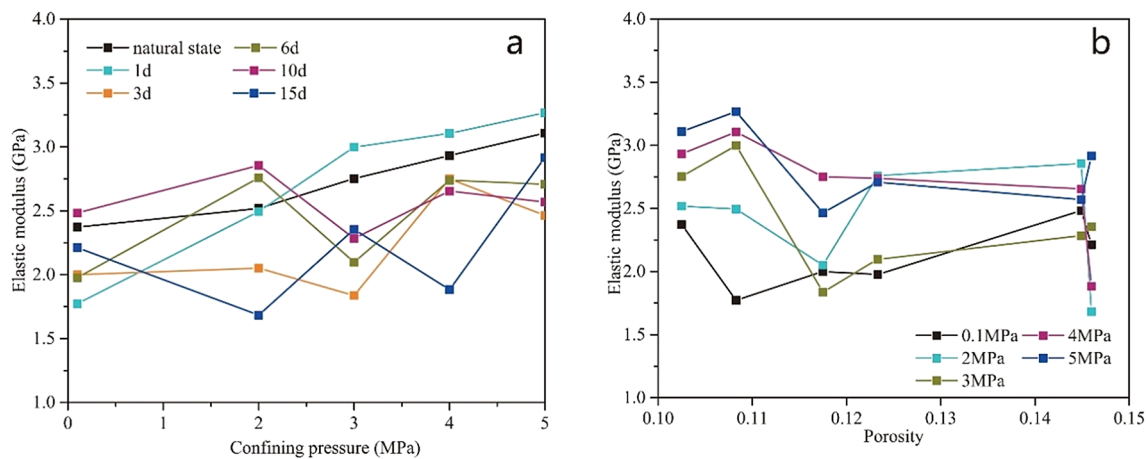


Fig. 7 Elastic modulus of samples according to confining pressure and porosity

different water–rock reaction times, with increasing confining pressure, the elastic grinding of rock samples showed an unstable increasing trend. When the confining pressure increased from 0.1 MPa to 5 MPa, the elastic modulus of the initial state sample increased by 31.02%, with the most notable increase (34.21%) occurring after 1 day of water–rock reactions and the lowest increase (3.54%) occurring after 10 days of water–rock reactions. Figure 7b shows the elastic modulus of rock samples according to porosity. Under different confining pressures, the elastic modulus showed an unstable decreasing trend with increasing porosity. When the porosity increased from 0.1025 to 0.1460, the maximum increase in elastic modulus was 35.79% at 4 MPa of confining pressure, and its minimum increase was 6.22% at 5 MPa of confining pressure.

It can be seen that the confining pressure tends to promote the increase of the elastic modulus of the samples, because the increase of the confining pressure leads to a better effect on the closure of the pores inside the samples. With the increase of dissolution time, the elastic modulus of the samples showed fluctuation with the increase of porosity; thus, we believe that there is no clear relationship between the change of elastic modulus and the porosity of the samples, which is consistent with the results of previous studies (Envelope et al. 2022). By further analyzing the changes in the macrostructure of the samples (Fig. 3), we conclude that the samples elastic modulus is mainly related to the spatial location and shape of the weak zones appearing in the samples, mainly due to the non-uniform spatial distribution of gypsum in different samples, which is an inevitable problem for natural samples (Yao et al. 2023).

3.2.4 Cohesion and Internal Friction Angle Variation with Water–Rock Reaction Time

The cohesion, c , and angle of internal friction, φ , reflect the ability of rock to resist shear deformation. By making the Mohr stress circle, the cohesion and internal friction angle of gypsum-bearing mudstone under water–rock reactions were obtained (Fig. 8).

As shown in Fig. 8a, the cohesion of the sample decreased linearly with increasing porosity ϕ_c . With the porosity increasing from 0.1083 to 0.1460, the sample cohesion decreased by 79.02%. By fitting with the experimental results, the relation between cohesion and porosity can be expressed as:

$$c(\phi_c) = -76.11\phi_c + 12.748, \quad (4)$$

where c is cohesion, MPa; ϕ_c is porosity, %.

Figure 8b shows the internal friction angle of the sample according to porosity. The angle did not change notably with porosity. After 10 days of dissolution, the internal friction angle of the sample was small. Before and after dissolution, the angle of internal friction of the samples was within the range of 35.29° and 37.76° , and the variation was not significant.

The cohesion and angle of internal friction are related to the cementation of particles within the rock and the way particles contact with each other (Baud et al. 2016). Under the water–rock reactions, water dissolves material along the crystal interface and mineral deconstruction surface, changing the way particles contact with each other, weakening the contact strength and generating intergranular dissolved pore (Fig. 4). These reduce the shear strength of the rock, which in the present study is mainly reflected in the deterioration

of the cohesion of the rock. It is worth noting that with the increase of dissolution time, the microstructure deterioration of the samples increases and the viscoelastic deformation capacity of the specimen gradually decreases (Yu et al. 2015; Fan and Teng 2007). This scenario is supported by the post-peak stress–strain curve of the sample during the viscoelastic deformation phase.

3.3 Construction and Verification of Constitutive Model

The analysis of the evolution of mechanical parameters and the deterioration mechanism of the samples under the water–rock reactions laid the foundation for the construction of the constitutive model.

3.3.1 Model Construction

Based on the statistical damage theory, a constitutive model of water–rock reaction relies on selecting the appropriate damage model, strength criterion, and strength probability model of rock microunits (Lemaitre 1984). We selected the widely used Drucker–Prager failure criterion, which has a simple parametric form, to measure the microelement strength (Li et al. 2012). Assuming that the strength of a microelement follows a Weibull distribution, the evolution equation of damage variables was calculated by integrating the probability density function, and the chemical damage variables were calculated according to the effective bearing area. Hence, the constitutive model of rock mechanics under water–rock reactions was obtained. The detailed derivation process is available in related studies (Lin et al. 2019; Xu et al. 2018; Feng et al. 2020).

$$\begin{cases} E_c = \left(1 - \left(\frac{\phi_c - \phi_0}{1 - \phi_0}\right)^{\frac{2}{3}}\right)E \\ \sigma_1 = \exp\left[-\frac{1}{F_0^m} \left(B_1 \varepsilon_1 + B_2 \frac{E_c \varepsilon_1 \sigma_3}{\sigma_1 - 2\mu\sigma_3}\right)^m\right] E_c \varepsilon_1 + 2\mu\sigma_3 \end{cases}, \quad (5)$$

where E and E_c are the elastic modulus of rock and that under water–rock reactions, respectively, ϕ_0 and ϕ_c are the initial porosity and porosity after water–rock reactions, respectively, σ_i is the nominal stress ($i = 1, 2, 3$), μ is Poisson's ratio, ε_1 is the axial deformation, and F_0 , and m are the parameters of the Weibull distribution.

In the constitutive model, E , E_c , σ_i , ϕ_0 , and ϕ_c are basic physical parameters that can be obtained through experiments. Given the simplicity of obtaining the solution and its clear physical meaning, we used the polar method to determine F_0 and m as follows (Lin et al. 2019):

$$m = \frac{-F_p}{\left(B_1 + B_2 \frac{E_c \sigma_3}{\sigma_p - 2\mu\sigma_3}\right) \varepsilon_p \ln(1 - D_{mp})}, \quad (6)$$

$$F_0 = F_p \left[-\ln(1 - D_{mp})\right]^{-\frac{1}{m}}, \quad (7)$$

where

$$B_1 = \left(\frac{1}{\sqrt{3}} + \alpha\right)E, \quad (8)$$

$$B_2 = \left[\left(2\alpha + \frac{2}{\sqrt{3}}\right)\mu + 2\alpha - \frac{1}{\sqrt{3}}\right], \quad (9)$$

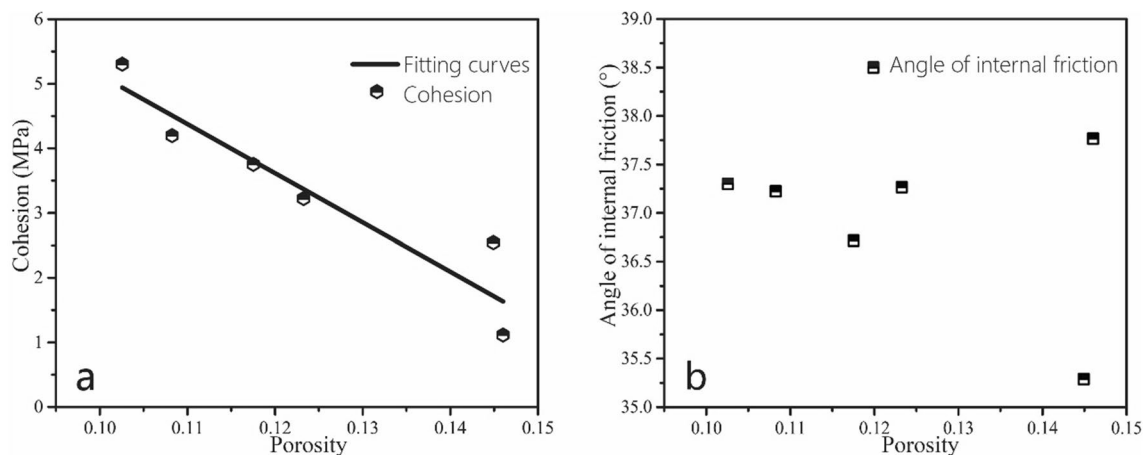


Fig. 8 Cohesion and internal friction angle of samples according to porosity

$$F_p = B_1 \varepsilon_p + B_2 \frac{E_c \varepsilon_p \sigma_3}{\sigma_p - 2\mu \sigma_3}, \tag{10}$$

$$\alpha = \frac{\sin \varphi}{\sqrt{9 + 3 \sin^2 \varphi}}, \tag{11}$$

and D_{mp} is the damage factor at the peak strength of the stress–strain curve, $D_{mp} = 1 - \frac{\sigma_p - 2\mu \sigma_3}{E \varepsilon_p}$.

From the analysis above, we know that σ_p and ε_p in the model change with confining pressure σ_3 and porosity ϕ_c . Parameters F_0 and m of the Weibull distribution can be found by substituting Eqs. (2) and (3) into Eq. (10) and then into Eqs. (6) and (7). Figure 9 shows the values of different sample Weibull distribution parameters. The variation of m increases with the time of water–rock reactions is not obvious, and the overall variation is small; F_0 fluctuates with the increase of water–rock reactions time, with the overall pattern of gradually decreasing with the increase of dissolution time. Parameters F_0 and m describe the stress–strain characteristics of gypsum-bearing mudstone under different surrounding pressure and dissolution time, providing a method to study the macroscopic mechanical behavior of the rock. However, the differences in the spatial location of the distribution of weak zones and the inadequate description of quantitative damage to the microstructure are important reasons for the fluctuation of parameters F_0 and m .

This way, we solved all the parameters in the constitutive structure model. Next, we verified the accuracy of the established model.

3.3.2 Model Verification

As shown in Fig. 10, the theoretical stress–strain curves under water–rock reactions and gypsum-bearing mudstone at different times are consistent with the experimental curves.

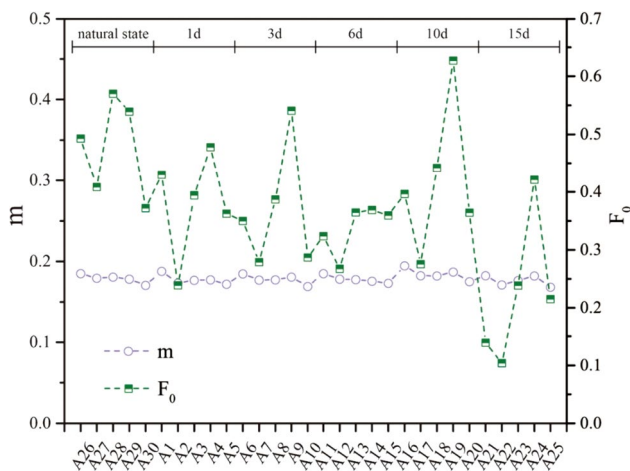


Fig. 9 Weibull distribution parameters F_0 and m

The theoretical model can well reproduce the variation characteristics of the stress–strain curve near the peak. However, in the elastic deformation stage of the sample, the predicted stress value of the model established in this paper is slightly larger than the measured value, and with the increase of the peripheral pressure, the stress value of the theoretical stress–strain curve is closer to the measured value. It is analyzed that, due to the influence of the spatial difference of gypsum distribution, the solution holes and cavities generated by dissolution cannot be closed well under the low circumferential pressure, which leads to a slightly worse fitting effect of the measured and theoretical stress–strain curves of the specimens under the low circumferential pressure. With the increase of the circumferential pressure, the solution holes and cavities generated inside the specimens are gradually closed, and the measured and theoretical stress–strain curves of the specimens at this time are gradually better fitted to the theoretical values, which also indicates that statistical damage is the main reason to use the theory as a measure for the stress of gypsum-containing mudslides. This also shows that there are some deficiencies in the statistical damage theory as the basis for measuring the dissolution damage of gypsum-bearing mudstone.

As can be seen from Fig. 10, the fitting effect between the theoretical curve and the measured curve in the early stage of dissolution is poor, and the difference between the theoretical curve and the measured curve gradually decreases with the increase of dissolution time. It is analyzed that, in the pre-dissolution period, with the rapid dissolution of gypsum and sodium sulfate, the weak zone of the samples mainly appeared in the location of the distribution of soluble salts, and this spatial variability is the main reason why the theoretical curve has a slightly poorer fitting effect with the measured curve. It is not practical to use field cores for indoor experiments to obtain samples with identical gypsum distribution. In the late stage of dissolution, the pores and cavities are gradually enlarged, some insoluble particles are detached, and the influence of the spatial difference of gypsum distribution on the mechanical properties of the specimens is gradually reduced. At this time, the measured stress–strain curves of the dissolved specimens are better fitted to the theoretical ones, which proves that the established intrinsic model is more suitable for describing the changes of the mechanical properties of gypsum-bearing mudstones under a long time of dissolution. From the overall fitting effect, it is considered that the damage constitutive model established in this study can basically be used to predict the changes in mechanical behavior of gypsum-bearing mudstone under dissolution and corrosion.

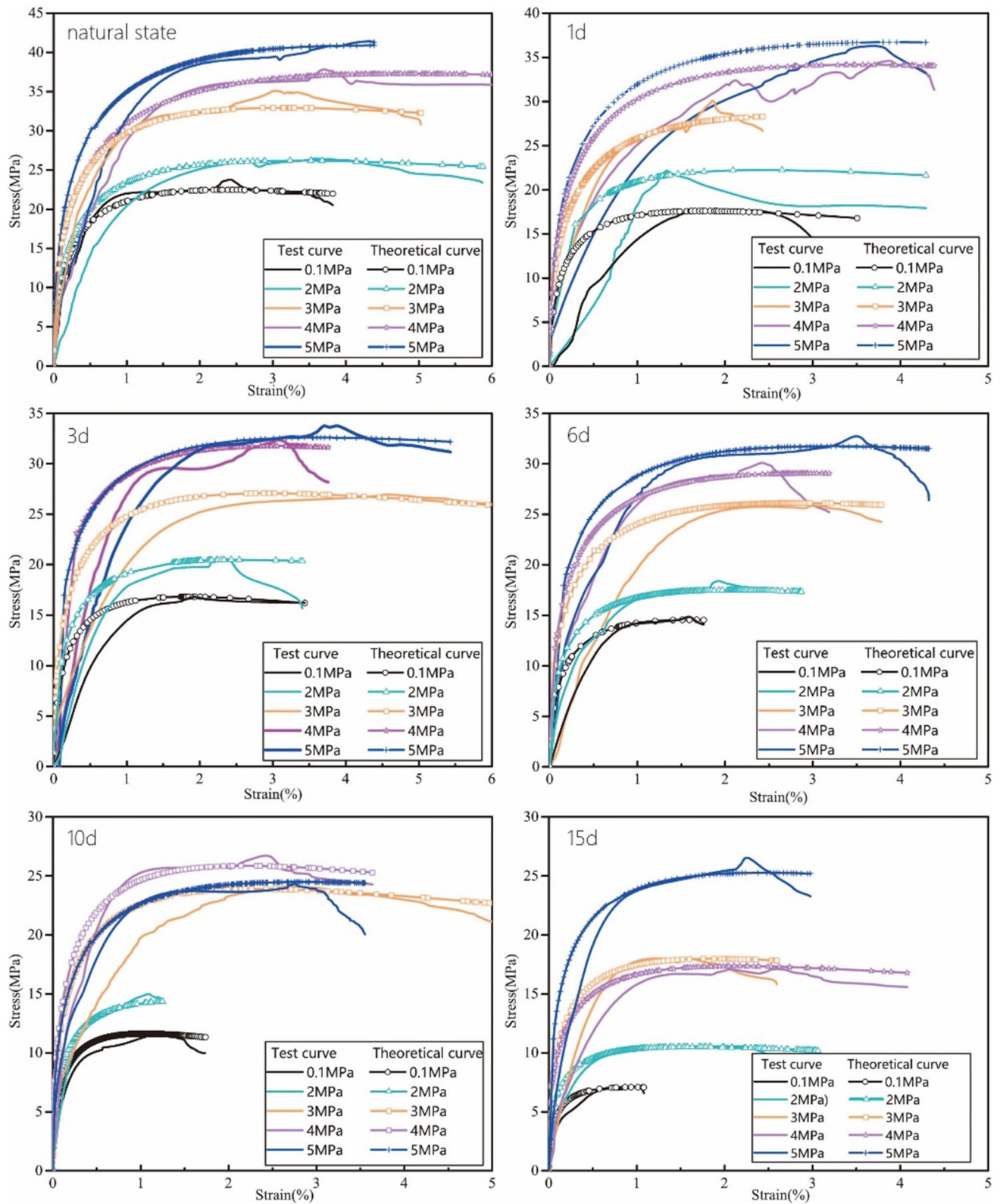


Fig. 10 Comparison between experimental data and theoretical model

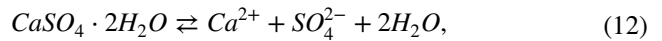
3.4 Discussion

3.4.1 Deterioration Mechanism of Mechanical Parameters of Samples Under Water–Rock Reactions

In summary, the results show that the water–rock reaction leads to the deterioration of the strength characteristics and deformation properties of gypsum-bearing mudstones, which is characterized by macroscopic and microscopic synergistic changes. Unlike the mudification, softening and lubrication of rock particles by the presence of water, the deterioration of rock mechanical properties by water–rock reactions is more attributable to irreversible structural damage, such as the weakening of microscopic particle connections and the appearance of macroscopic defect zones. Gypsum-bearing mudstone is a composite material composed of two or more materials with different chemical or physical properties (Fig. 11a) and exhibits complex mechanical behavior in the water–rock reactions.

Specifically speaking, groundwater enters the interior of the gypsum-bearing mudstone through the pore space, resulting in the dissolution of gypsum (Eq. 12), sodium sulfate (Eq. 13), and the shedding of a few insoluble particles (Fig. 11b), which is manifested as the reduction of the mass of the gypsum-bearing mudstone and the increase of porosity. The increase of porosity means that the volume of gypsum-bearing mudstone decreases, and the peak strength of the specimen gradually decreases; unlike the effect of porosity on peak strength, the change of the tangent of the

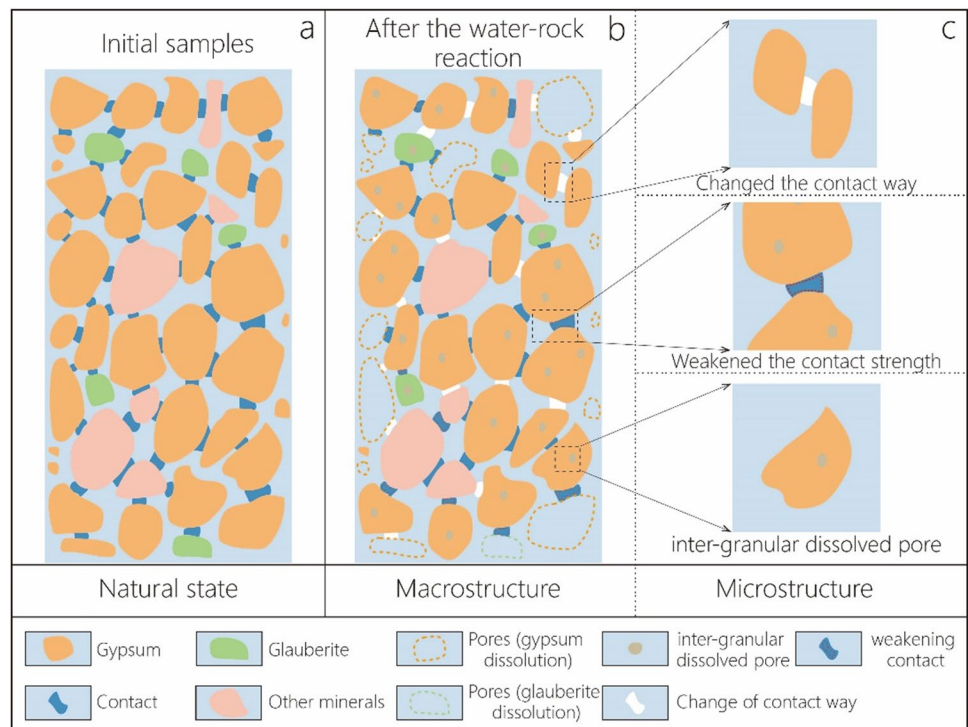
stress–strain curve of the samples shows a stronger causal relationship with the location of the weak zone. Confining pressure has a facilitating effect on the peak strength and modulus of elasticity of the samples, due to the gradual closure of the pores as the confining pressure increases. The cohesion of the samples decreases negatively and linearly with the increase of porosity, while the internal friction angle shows fluctuating changes, in which the change and weakening of microscopic contact between particles and the appearance of intergranular dissolved pores play an important role (Fig. 11c).



3.4.2 Scope for Future Study

The objective of this paper is to develop a construction model that can accurately predict the mechanical softening behavior of gypsum-bearing mudstone after water–rock reaction. Compared with previous studies, we not only explore the variation of elastic modulus, cohesion and internal friction angle, but also the relationship between peak intensity and confining pressure and dissolution degree, which broadens the applicability of the model in this paper. The comparison between the theoretical curve and the measured model reveals that the model gives a better

Fig. 11 Deterioration mechanism of the mechanical properties



prediction of the viscoelastic deformation characteristics in the gypsum stress–strain curve. However, the theoretical curves do have some errors with the measured curves. It indicates that there are some defects in explaining the mechanical behavior of gypsum under the water–rock reactions from macroscopic mechanical properties.

For the reason of this discrepancy, we believe it is caused by the still unclear research on how microstructure affects the mechanical properties of gypsum and the microphysical processes of gypsum deformation and damage. In this paper, our objective is to elucidate the impact of water–rock reactions on the microstructure of gypsum using scanning electron microscopy (SEM) and to gain insights into these processes, and we have achieved some understanding. However, we were unable to characterize this cause-and-effect relationship through mathematical relationships, resulting in the inability to establish a quantitative relationship between microstructural changes and the evolution of macroscopic mechanical properties. This results in the analysis of the change pattern of mechanical parameters of gypsum. Therefore, we believe that studying the mechanical properties of gypsum under the water–rock reaction from a macroscopic point of view is not helpful to predict its real mechanical behavior. In the future, the influence of microstructure and fine mechanisms on macroscopic mechanical properties should be explored in depth, and the macroscopic constitutive relationship of gypsum should be constructed from the interaction between microscopic particles.

4 Conclusion

A comprehensive understanding and proper estimation of gypsum-bearing rock strength and deformation behaviors during water–rock reactions are of great significance for underground engineering construction. We conducted a series of indoor dissolution tests and mechanical tests to explore the evolution law and mechanism of strength and deformation parameters of gypsum-bearing mudstone. On the basis of in-depth analysis of the test results, a mechanical constitutive model was constructed, which fitted well the indoor measured data. The following conclusions can be drawn from this study:

1. Water–rock reactions are inducing factors for changes in gypsum-bearing mudstone strength and deformation properties. During reaction, the porosity of gypsum-bearing mudstone increases.
2. The effect of water–rock reactions on the microstructure of gypsum-bearing mudstone is reflected in the weakening of particle contact, which changes the contact

pattern between particles, and various microdefects grow to form weak zones weak areas. This is the reason for the substantial deterioration of rock mechanical properties.

3. Water–rock reactions reduce the peak strength, and cohesion of gypsum-bearing mudstone, and the enclosing pressure has a facilitating effect on the peak strength and elastic modulus of rock. Water–rock reactions have less effect on the internal friction angle of gypsum-bearing mudstone. For samples with different shapes and spatial locations of weak zones due to water–rock reactions, there is no clear relationship between the change of elastic modulus and the porosity of the samples.
4. By constraining the peak strength and peak deformation, the established constitutive model of gypsum-bearing mudstone is accurate and flexible. In the future research, the study of microstructural changes of gypsum under water–rock reactions should be strengthened, and the macroscopic constitutive relationship of gypsum should be constructed from the interaction between microscopic particles.

Acknowledgements This study was supported by the National Natural Science Foundation of China (U2244215; No. 42072280; No. 42202292), Chengdu Multi-factor City Geological Survey (DD20189210) and Comprehensive Geological Survey of Resources and Environment in the Cheng-Mian-Le Development Zone of the Shuangcheng Economic Circle in the Chengdu-Chongqing Area (DD20211402).

Data availability The data that support the findings of this study are available from the corresponding author upon reasonable request.

References

- Adams RI, Chen W, Kumagai K, Macher JM, Mendell MJ (2019) Relating measured moisture of gypsum board to estimated water activity using moisture meters. *Build Environ* 147:284–298
- Bajni G, Apuani T, Beretta GP (2019) Hydro-geotechnical modelling of subsidence in the Como urban area. *Eng Geol*. 257:105144
- Barbero EJ, Vivo LD (2001) A constitutive model for elastic damage in fiber-reinforced PMC laminae. *Int J Damage Mech* 10(1):73–93
- Baud P, Rolland A et al (2016) Impact of stylolites on the mechanical strength of limestone. *Tectonophysics Amsterdam*. 690:4–20
- Bertotti G, Mosca P (2009) Late-orogenic vertical movements within the arc of the SW Alps and Ligurian Alps. *Tectonophysics* 475(1):117–127
- Bonetto S, Fiorucci A, Fornaro M, Vigna B (2008) Subsidence hazards connected to quarrying activities in a karst area: the case of the Moncalvo sinkhole event (Piedmont, NW Italy). *Estonian J Earth Sci* 57(3):125–134
- Brantley SL, Conrad CF (2008) Kinetics of Water–Rock Interaction: Kinetics of Water–Rock Interaction

- Criss RE, Nelson DL (2020) Discharge-Stage relationship on Urban streams evaluated at USGS Gauging Stations, St. Louis, Missouri. *J Earth Sci* 31(6):9
- Cristallini EO, Ramos VA (2000) Thick-skinned and thin-skinned thrusting in the La Ramada fold and thrust belt: crustal evolution of the High Andes of San Juan, Argentina (32 SL). *Tectonophysics* 317(3–4):205–235
- David EC, Brantut N, Schubnel A, Zimmerman RW (2012) Sliding crack model for nonlinearity and hysteresis in the uniaxial stress–strain curve of rock. *Int J Rock Mech Min Sci* 52:9–17
- Envelope C, Pb B, Arlkb C, Tr B, Smrb A (2022) Influence of water on deformation and failure of gypsum rock. *J Struct Geol* 163:104722
- Fan C, Teng HH (2007) Surface behavior of gypsum during dissolution. *Chem Geol* 245:242–253
- Feng WL, Qiao CS, Wang T, Yu MY, Jia ZQ (2020) Strain-softening composite damage model of rock under thermal environment. *Bull Eng Geol Env* 79:4321–4333
- Gao F, Xiong X, Xu C, Zhou K (2021) Mechanical property deterioration characteristics and a new constitutive model for rocks subjected to freeze-thaw weathering process. *Int J Rock Mech Min Sci* 140:104642
- Gong F, Yan J, Li X, Luo S (2019) A peak-strength strain energy storage index for rock burst proneness of rock materials. *Int J Rock Mech Min Sci* 117:76–89
- Homand GF (2005) Modelling long-term behaviour of a natural gypsum rock. *Mech Mater* 37:1223–1241
- Hoxha D, Homand F, Auvray C (2006) Deformation of natural gypsum rock: mechanisms and questions. *Eng Geol* 86(1):1–17
- Işık Y (2010) Influence of water content on the strength and deformability of gypsum. *Int J Rock Mech Min Sci* 47:342–347
- Juang CH (2021) BFTS - engineering geologists' field station to study reservoir landslides. *Eng Geol* 284(4):106038
- Lafrance N, Auvray C et al (2016) Impact of weathering on macro-mechanical properties of chalk: Local pillar-scale study of two underground quarries in the Paris Basin. *Eng Geol* 203:107–119
- Lemaître J (1984) How to use damage mechanics. *Nucl Eng Des* 80:233–245
- Li X, Cao W-G, Su Y-H (2012) A statistical damage constitutive model for softening behavior of rocks. *Eng Geol* 143:1–17
- Li X, Peng K, Peng J, Hou D (2021) Experimental investigation of cyclic wetting-drying effect on mechanical behavior of a medium-grained sandstone. *Eng Geol* 293:106335
- Liang W, Yang X, Gao H, Zhang C, Zhao Y, Dusseault MB (2012) Experimental study of mechanical properties of gypsum soaked in brine. *Int J Rock Mech Min Sci* 53:142–150
- Lin Y, Zhou K, Gao F, Li J (2019) Damage evolution behavior and constitutive model of sandstone subjected to chemical corrosion. *Bull Eng Geol Env* 78:5991–6002
- Lisabeth HP, Zhu W (2015) Effect of temperature and pore fluid on the strength of porous limestone. *J Geophys Res Solid Earth*. 120:6191–9208
- Liu Y, Dai F (2018) A damage constitutive model for intermittent jointed rocks under cyclic uniaxial compression. *Int J Rock Mech Min Sci* 103:289–301
- Liu XS, Ning JG et al (2016) Damage constitutive model based on energy dissipation for intact rock subjected to cyclic loading. *Int J Rock Mech Mining Sci*. 85:27–32
- Liu B, Yang H, Karekal S (2020) Effect of water content on Argillization of mudstone during the tunnelling process. *Rock Mech Rock Eng* 53(2):799–813
- Ma H, Song Y, Chen S, Yin D, Ma Q (2021a) Experimental investigation on the mechanical behavior and damage evolution mechanism of water-immersed gypsum rock. *Rock Mech Rock Eng* 54:4929–4948
- Ma H, Song Y, Chen S et al (2021b) Experimental investigation on the mechanical behavior and damage evolution mechanism of water-immersed gypsum rock. *Rock Mech Rock Eng* 54(9):4929–4948
- Meng T, Hu Y, Fang R, Fu Q, Yu W (2016) Weakening mechanisms of gypsum interlayers from Yunying salt cavern subjected to a coupled thermo-hydro-chemical environment. *J Natl Gas Sci Eng* 30:77–89
- Miao S, Cai M, Guo Q, Wang P, Liang M (2016) Damage effects and mechanisms in granite treated with acidic chemical solutions. *Int J Rock Mech Min Sci* 88:77–86
- Niu Q, Wang Q, Wang W et al (2022) Responses of multi-scale microstructures, physical-mechanical and hydraulic characteristics of roof rocks caused by the supercritical CO₂–water–rock reaction. *Energy* 238:121727
- Nol C, Baud P, Violay M (2021) Effect of water on sandstone's fracture toughness and frictional parameters: Brittle strength constraints. *Int J Rock Mech Min Sci* 147:104916
- Ping S, Wang F, Wang D, Li S, Yuan Y, Feng G, Shang S (2023) Multi-scale deterioration mechanism of shear strength of gypsum-bearing mudstone induced by water-rock reactions. *Eng Geol* 323:107224
- Sadeghiamirshahidi M, Vitton SJ (2019) Laboratory study of gypsum dissolution rates for an abandoned underground mine. *Rock Mech Rock Eng* 52:2053–2066
- Sammis CG, Ashby MF (1986) The failure of brittle porous solids under compressive stress states. *Acta Metall* 34(3):511–526
- Song K, Wang F, Yi Q, Lu S (2018) Landslide deformation behavior influenced by water level fluctuations of the Three Gorges Reservoir (China). *Eng Geol*. 247:58–68
- Voyiadjis GZ, Kattan PI (2009) A comparative study of damage variables in continuum damage mechanics. *Int J Damage Mech* 18:315–340
- Wang X, Crupi V, Jiang C, Feng ES, Guglielmino E, Wang CS (2017) Energy-based approach for fatigue life prediction of pure copper. *Int J Fatigue* 104:243–250
- Wei DY, Wei GL, Yan RL, Yan MY (2015) The meso-mechanism study of gypsum rock weakening in brine solutions. *Bull Eng Geol Env* 75(1):1–9
- Wong L, Einstein HH (2009) Systematic evaluation of cracking behavior in specimens containing single flaws under uniaxial compression. *Int J Rock Mech Min Sci* 46(2):239–249
- Xu X, Gao F, Zhang Z (2018) Thermo-mechanical coupling damage constitutive model of rock based on the Hoek-Brown strength criterion. *Int J Damage Mech* 27:1213–1230
- Yao W, Li C, Zhan H, Zhou JQ, Jiang X (2020) Multiscale study of physical and mechanical properties of sandstone in three gorges reservoir region subjected to cyclic wetting-drying of yangtze river water. *Rock Mech Rock Eng* 53:2215–2231
- Yao W, Li C, Ke Q et al (2023) Multi-scale deterioration of physical and mechanical properties of argillaceous siltstone under cyclic wetting-drying of Yangtze River water. *Eng Geol* 312:106925
- Yu WD, Liang WG, Li YR, Yu YM (2015) The meso-mechanism study of gypsum rock weakening in brine solutions. *Bull Eng Geol Env* 75:1–9
- Yun L, Gao F, Zhou K, Gao R, Guo H (2019) Mechanical properties and statistical damage constitutive model of rock under a coupled chemical-mechanical condition. *Geofluids* 2019(6):1–17
- Zhu C, Xu X et al (2019) Softening damage analysis of gypsum rock with water immersion time based on laboratory experiment. *IEEE Access*. 7:125575
- Zhu C, Karakus M, He M et al (2022) Volumetric deformation and damage evolution of Tibet interbedded skarn under multistage constant-amplitude-cyclic loading. *Int J Rock Mech Min Sci* 152:105066
- Zucali M, Barberini V, Chateigner D, Ouladdiaf B, Lutterotti L (2010) Brittle plus plastic deformation of gypsum aggregates experimentally deformed in torsion to high strains: quantitative

microstructural and texture analysis from optical and diffraction data. *Geol Soc London Spec Public.* 332:79–98

Publisher's Note Springer Nature remains neutral with regard to jurisdictional claims in published maps and institutional affiliations.

Springer Nature or its licensor (e.g. a society or other partner) holds exclusive rights to this article under a publishing agreement with the author(s) or other rightsholder(s); author self-archiving of the accepted manuscript version of this article is solely governed by the terms of such publishing agreement and applicable law.